Aqueous chemical solution deposition of ultra high-k LuFeO3 thin films

Peer-reviewed author version

GIELIS, Sven; Ivanov, Maksim; PEYS, Nick; VAN DEN HAM, Jonathan; PAVLOVIC, Nikolina; Banys, Juras; HARDY, An & VAN BAEL, Marlies (2017) Aqueous chemical solution deposition of ultra high-k LuFeO3 thin films. In: JOURNAL OF THE EUROPEAN CERAMIC SOCIETY, 37(2), p. 611-617.

DOI: 10.1016/j.jeurceramsoc.2016.08.042
Handle: http://hdl.handle.net/1942/22811

Aqueous chemical solution deposition of ultra high-*k* $LuFeO_3$ thin films

Sven Gielis[1], Maksim Ivanov[2], Nick Peys[1], E. Jonathan van den Ham[1], Nikolina Pavlovic[1], Juras Banys[2], An Hardy[1], Marlies K. Van Bael[1]

1 Hasselt University, Institute for Materials Research and IMEC vzw, Division IMOMEC, Inorganic and Physical Chemistry, Diepenbeek, Belgium

2 Vilnius University, Faculty of Physics, Vilnius, Lithuania

Abstract

Thin orthorhombic ultra high-*k* $LuFeO_3$ (LFO) films on $Si_3N_4/SiO_2/Si$ substrates were obtained by means of aqueous chemical solution deposition (CSD). Prior to thin film deposition, the precursor synthesis, thermal decomposition and crystallization behavior of the bulk material were studied. It was shown that phase-pure hexagonal LFO powder could be formed at 650°C while a higher temperature of 900°C was required to obtain the orthorhombic phase. Deposition on SiO_2/Si resulted in the development of silicates in this temperature range, thus preventing the formation of the orthorhombic $LuFeO_3$ phase. The use of $Si_3N_4/SiO_2/Si$ as the substrate shifted the silicate formation to higher temperature, allowing the synthesis of phase-pure orthorhombic $LuFeO_3$ as a thin film at 1000°C. Impedance spectroscopy analyses confirmed its associated ultra high dielectric constant (> 10000) at room temperature for frequencies lower than or equal to 1 kHz.

Introduction

Ultra high-*k* materials are very attractive for applications in the field of energy storage, which has recently attracted great attention.[1–3] Thin film capacitors store their energy in a thin layer of dielectric material which is sandwiched between two highly conductive layers. The amount of energy stored in the stack is proportional to the capacitance of the dielectric film.[4] Consequently, the use of an oxide with a giant dielectric constant can increase the energy density and thus allows the miniaturization of these energy storage devices, yielding ultracapacitors.[1] For orthorhombic $LuFeO_3$ (o-LFO) ceramics in the bulk state, a dielectric constant of ca. 10^4 (frequency ≤ 1kHz) has been reported at room temperature. [5,6] This is much higher compared to the other abundant crystalline form, i.e. hexagonal $LuFeO_3$ (h-LFO), which has a *k*-value of only 3.10^2 (frequency ≤ 1kHz) at room temperature.[7] However, it is mainly due to the latter crystalline phase that $LuFeO_3$, a member of the rare-earth orthoferrites family, has attracted considerable attention in recent years. Hexagonal LFO has promising multiferroic, magnetic and optical properties which can be used for next generation applications in information technology, sensing and actuation. [5,8–12] Experimental results suggest that h-LFO is both ferroelectric and antiferromagnetic at room temperature. Since it is one of the only few known room-temperature multiferroics, its potential towards practical applications is very large.[5,7,9,13] Hence, the synthesis of bulk h-LFO via solid-state reactions is well described in literature.[5,6,14] Also the deposition of thin films has been reported, in particular using pulsed laser deposition [7–9], metal-organic chemical vapor deposition [7], molecular-beam epitaxy (MBE) [13] and sol-gel chemistry [7], as well as the exact characteristics of h-LFO such as the morphology and its multiferroic properties.

Orthorhombic LFO has been much less investigated in the past, only reports concerning the study of bulk o-LFO could be found.[5,6] This is because this perovskite oxide is not ferroelectric and thus not interesting for multiferroic applications. However, as mentioned, we selected o-LFO and, particularly, as thin film because of its great potential when it comes to energy storage applications. Literature on the deposition of ultra high-*k* o-LFO thin films is even more scarcely available. The deposition of an o-

LFO film on $LaNiO_3$/Si via pulsed laser deposition has been shown, however the dielectric constant of the layer was not reported.[15]

Here, we report the development of a novel aqueous chemical solution (CSD) process for the deposition of o-LFO thin films. This route is known to allow the fabrication of complex multi-metal oxides due to the intimate mixing of metal ions and the resulting good homogeneity of the precursor which consists of environmentally friendly water instead of organic solvents [16–18] It was shown before that citrato-complexes of several lanthanides (i.e. Nd, Pr, Eu, Sm, Gd) in water can be successfully synthesized and that these precursors are useful for the deposition of oxide films. [19,20] Furthermore it was proven by Hardy et al. and Van Elshocht et al. that the dielectric constant of CSD thin films is equal to that of films from other deposition techniques, such as atomic layer deposition.[16,17]

Materials and methods

Aqueous Lu/Fe precursor and Lu/Fe oxide powder synthesis

As can be seen in Figure 1, first, the mono-metal Fe (III) and Lu (III) ion solutions were prepared separately. The Fe (III) precursor, which was synthesized as reported earlier by refluxing the required Fe (III) citrate hydrate ($FeC_6H_5O_7.H_2O$, 98%, 18-20% Fe, Acros) in water at 80°C overnight, had a concentration of 0.1 mol/l. [21] For the Lu (III) precursor, Lutetium (III) oxide (Lu_2O_3, 99.9%, Alfa Aesar) and citric acid ($C_6H_8O_7$, 99%, Sigma-Aldrich) were added in a minimal amount of water (citric acid to Lu^{3+} = 1:1) and refluxed for 24h at 120°C. The pH was raised to 11 with concentrated ammonia (NH_3, extra pure, 32%, Merck) after which the mixture was refluxed again for 24h at 110°C, finally yielding a clear, colorless 0.1 M solution, with a pH of about 7.5. The mono-metal ion precursor solutions were filtered using a membrane filter (Nalgene, 0.2 µm) to remove particles, such as dust, impurities and undissolved fractions. Subsequently their exact concentration was determined by inductively coupled plasma atomic emission spectroscopy ICP-AES (Optima 3000, PerkinElmer). The multi-metal ion precursor for $LuFeO_3$ was prepared by mixing the Fe (III) and Lu (III) solutions in the desired ratio so that the total metal ion concentration was 0.1 M.

For the powder synthesis, first, the solvent of the precursor solution was evaporated in air at 80°C to allow gelation. The obtained gel was then crushed and ground manually in an agate mortar before further thermal treatment in view of crystallization. The decomposition of the gel was studied by means of a simultaneous thermal gravimetric (TG) / differential scanning calorimetry (DSC) analysis in a TA Instruments SDT Q600. The gel (±4 mg of sample) was heated from room temperature to 1000°C at a heating rate of 10°C min^{-1} in dry air (100 ml min^{-1}). The crystallization behavior of Lu/Fe powder, which was precalcined at 200°C for 30 minutes, versus temperature was studied in-situ by HT-XRD (high-temperature X-ray diffraction, Bruker D8, step size 0.02°2θ). The measurements were carried out between 10 and 60°2θ at a heating rate of 10°C/min, with 30 min intervals of 50°C from 500 to 1100 °C.

Thin Lu/Fe oxide film deposition

Thin films were deposited via spin coating (3000 rpm, 30 s) of the Lu/Fe multi-metal ion precursor onto pieces (ca. 2.5 x 2.5 cm^2) of SiO_2/Si (100) (1.2 nm SiO_2) and Si_3N_4/SiO_2/Si (70 nm Si_3N_4/1.2 nm SiO_2).

To allow deposition of uniform films, the SiO_2/Si and Si_3N_4/SiO_2/Si substrate surfaces were first cleaned. For the SiO_2/Si stack, this was done by cleaning in SPM (sulfuric acid mixture, consisting of 4:1 H_2SO_4 (p.a., 95-97%, Merck) : H_2O_2 (stabilized p.a., 35%, Acros Organic)) followed by an APM treatment (ammonia peroxide mixture, 5:1:1 H_2O : H_2O_2 (stabilized p.a., 35%, Acros Organic): NH_3 (extra pure, 32%, Merck)).[22] The Si_3N_4/SiO_2/Si surface was pretreated in a UV/O_3 environment at 60°C for 30 minutes.[23]

Multiple layers were deposited on the substrates, after each layer the sample was thermally treated using hot plate steps (based on the thermal gravimetric analysis, i.e. 1 min at 110°C, 2 min at 320°C and 2 min at 510°C) to decompose the precursor. The complete stack was further annealed for 30 minutes (heating rate of 10°C/min) in dry air (100 ml min^{-1}) using a furnace (post deposition anneal - PDA) to induce crystallization.

Film thicknesses were determined by ellipsometry (Plasmos, single wavelength) using a refractive index of 2.00 for a single layer model, and verified by means of cross-section scanning electron microscopy (X-SEM, FEI, NOVA 200) in secondary electron imaging mode. The film morphology was visualized in a tilted view (45°). The Lu/Fe thin film oxide phase formation was determined by X-Ray Diffraction (XRD) on a PANalytical X'pert Pro tool with Cu Kα radiation in a Bragg-Brentano configuration (coupled θ-2θ scan) with a PIXcel detector in scanning mode (step size 0.0098°). Possible silicate formation was detected by grazing angle attenuated total reflectance Fourier transform infrared (GATR-FTIR) spectroscopy. It was carried out using a 65° single reflection Ge-ATR (Harrick), placed inside the sample compartment of an FTIR spectrometer (Bruker,Vertex 70, 36 scans). To ensure intimate contact between the sample and the Ge-crystal, 0.4 Nm of torque was applied.

The dielectric constant was determined via impedance spectroscopy using a HP LCR meter 4284A (20 Hz – 1 MHz) at room temperature. Therefore, Au electrodes were deposited on the films as

interdigitated finger structures by means of a standard lithographic method. The interdigitated finger structure is characterized by 24 lanes (or fingers). The lanes are 1910 µm long and have a width of 17 µm, they are separated by 23 µm. The dielectric permittivity was determined using the model proposed by Kidner et al.[24] A substrate with deposited contacts of the same geometry was measured to account for the electrical properties of the substrate.

Results and discussion

Aqueous Lu/Fe precursor and Lu/Fe oxide powder synthesis

Information about the thermal decomposition of the precursor was gathered by a thermal gravimetric study (TGA/DSC) of a gel powder, obtained via evaporating water out of the precursor. In the precursor's decomposition profile, which is shown in Figure 2 and is similar to earlier reported metal-citrate gels [25–27], a small weight loss till 150°C can be observed. This decrease in weight can be ascribed to the evaporation of water, still present in the gel after precalcination or adsorbed afterwards. This step, known as the drying step, is followed by an abrupt weight loss, initiated at 180°C. This can be explained by the partial decomposition of the ammonium citrate gel matrix. Then, around 350°C, the decomposition of the direct coordination sphere of the metal ions is initiated, further shown by strongly exothermic processes at 400°C and 800°C, due to the removal of organic residual fractions and probably thermostable Lutetium dioxymonocarbonate, $Lu_2O_2CO_3$ which was confirmed by GATR-FTIR of deposited films (see Thin Lu/Fe oxide film deposition).[25–27]

The crystallization behavior of $LuFeO_3$ was studied on gel powders and followed using high-temperature XRD, allowing in-situ study of the phase (trans)formation during heating (10°C/min, air). As indicated before, the crystal structure of LFO is of high importance in function of energy storage applications since it is known that giant k-values can only be achieved in o-LFO.[5–7] For convenience, only the in-situ XRD patterns from 650°C and up are presented in Figure 3, no crystallization seems to occur till 650°C. From this temperature on, the formation of h-LFO phase can be observed in the XRD pattern, no secondary phases are detected. Then, from 700°C the onset of the formation of the o-LFO phase is noticeable. Between 700°C and 850°C both o-LFO and h-LFO are present in the powder: the signal intensities of o-LFO diffractions increase as the peak intensities of the hexagonal phase decrease and eventually fade away at 900°C. This indicates that, in this temperature range, the hexagonal phase transforms into the more thermodynamically stable orthorhombic phase. Consequently, an anneal at 900°C results in phase-pure o-$LuFeO_3$ powder. No secondary phases are developed by further

increasing the temperature (till 1100°C). The obtained o-LFO phase is maintained after cooling the sample down to room temperature.

It can be concluded that the presented aqueous citrate precursor allows the crystallization of both the phase-pure hexagonal and orthorhombic $LuFeO_3$ crystalline powders. It should be noted that for the latter, interesting for the described energy storage applications, high temperatures seem necessary to form the phase.

Thin Lu/Fe oxide film deposition

Based on the Lu/Fe precursor study, three hot plate (HP) steps were defined to allow gel decomposition and carbon removal out of the layer after each cycle of spin coating: (1) a hot plate step was set at 110°C for 1 minute to evaporate the water in the film, (2) another at 320°C for 2 minutes and (3) a last one at 510°C for 2 minutes. By using HP steps over a furnace treatment, we avoid the formation of cracks when gases escape from the interior and break through the skin.[19]

In this way, amorphous Lu/Fe oxide films were obtained on SiO_2/Si, a common substrate in semiconductor industry. Figure 4 shows that the Lu/Fe oxide film thickness, determined by ellipsometry (a) of which the model was checked by X-SEM (b), can be well controlled by varying the amount of deposition cycles. The films are very smooth after deposition (see SEM image) and the resulting film thickness varies linearly with the amount of cycles (see plot), so no semi-etching of the previous layer by the precursor occurs. [28] The intersection at the y-axis can be attributed to the 1.2 nm SiO_2 which is present on the silicon substrate.

To investigate the phase formation of the films on SiO_2/Si, 30 layers were spin coated resulting in a film thickness of ca. 130 nm (X-SEM), confirming the linear fit in Figure 4. These films were further treated for 30 min in a furnace (post deposition anneal in air, 10°C/min) in order to crystallize. The XRD results in Figure 5 show that 700°C is too low for the films to trigger the crystallization: an amorphous Lu/Fe oxide film is present after the heat treatment. A post deposition anneal at 800°C is necessary to initiate the crystallization of the film: a h-LFO film is obtained at this temperature. It can be inferred that the

crystallization temperature for LFO films is much higher compared to powders (650°C). This can be explained by an increase in activation energy for the crystallization of thin films compared to bulk material, considering volume induced crystallization.[29] Increasing the PDA temperature of the films to 900°C results in stronger signal intensities of the hexagonal phase, however also traces of $Lu_2Si_2O_7$ can be found in the XRD pattern. The presence of this silicate is very plausible since it is known that rare earth oxides tend to form silicates in contact with SiO_2 at high temperatures.[20,30] At 1000°C $Lu_2Si_2O_7$ takes the upper hand and $LuFeO_3$ is not present anymore in the film, instead, hexagonal Fe_2O_3 seems to be formed. At 1100°C the effect is even more pronounced.

Further proof of silicate formation in these films at high temperatures can be found in the GATR spectra in Figure 6. The longitudinal (LO) and transverse (TO) optic vibration of SiO_2, originating from the silicon substrate, are positioned at respectively 1240 cm^{-1} and 1065 cm^{-1}.[31] In the 1000-600 cm^{-1} region, the bands originate from the metal-oxygen stretching of Lu-O/Fe-O. Starting at 800°C and very clear at 1000°C and 1100°C there is a change in the bands in this region. A set of intense peaks appears in the GATR spectrum between 1020 and 780 cm^{-1}. This set, including the intense peak at approximately 1100 cm^{-1}, is indicative of rare earth silicate structures, thus confirming the formation of $Lu_2Si_2O_7$ in the film.[32,33] Since GATR is able to detect amorphous silicates [34] and thus complementary to XRD, one can understand that already at 800°C silicate formation, being amorphous, could be observed. These silicates turn crystalline by elevating the PDA temperature (see XRD).

From the GATR study in Figure 6 it is also clear that after a PDA at 700°C Lutetium dioxymonocarbonate species are still present in the film, indicated by the double peak at 1550 cm^{-1} and 1400 cm^{-1}.[35,36] Higher anneal temperatures are thus necessary to remove all carbon containing species, which was already indicated by the TG analysis of the gel (see Figure 2). Furthermore, CO_2/CO can be seen at 2350 cm^{-1} at 700-800°C, which is probably adsorbed from the air as well during as after the thermal treatment.[36]

The silicate crystallization at high temperatures can also be linked to the film morphology, as can been seen from the SEM images (tilted view, 45°) in Figure 7. The Lu/Fe oxide films after a post deposition

anneal at 800°C (A) and 900°C (B) have a rather smooth morphology. This drastically changes when further increasing the temperature to 1000°C (C) and 1100°C (D): these films are quite rough, indicating phase formation and accompanying interaction with the substrate, i.e. the crystallization of $Lu_2Si_2O_7$ in the film.

In order to study the LFO crystallization independently from interfacial reactions with the substrate, $Si_3N_4/SiO_2/Si$ was applied as a substrate. The Si_3N_4 layer is known for its chemical inertness and high thermal stability [37,38], and should act here as a protection layer against silicate formation. Via spin coating and accompanied hot plate treatment 65 nm Lu/Fe oxide films were deposited on $Si_3N_4/SiO_2/Si$. These samples were further treated for 30 min in a furnace (post deposition anneal in air, 10°C/min) in order to crystallize. Again, a temperature of 800°C is necessary to trigger the crystallization, it results in h-LFO as primary phase and o-LFO as secondary phase (XRD data not shown). However, a phase-pure orthorhombic $LuFeO_3$ film can be obtained by annealing the film at 1000°C in air. When increasing the temperature to 1100°C, the $Lu_2Si_2O_7$ signals appear in the XRD pattern and the o-LFO loses peak intensity. GATR analysis of these films was performed to detect silicate formation even before crystallization (see Figure 8). The signals at 815 cm^{-1} and 875 cm^{-1} are related to absorbance by stretching vibrations of the Si–N bonds [38–41], whereas the peak at 1080 cm^{-1} can be attributed to the stretching vibration of SiO_2.[40] In the 1000-600 cm^{-1} region, the other bands basically originate from the metal-oxygen vibrations of Lu-O/Fe-O. It seems that there is no change in bands in this region up to 1000°C. No other intense peaks seem to form, thus confirming that there is no silicate formation on the Si_3N_4 substrate and that a phase-pure o-LFO film can be formed by a PDA at 1000°C. However when increasing the anneal temperature to 1100°C, other signals in this region seem to appear, at the same position as the films on SiO_2/Si, indicating silicate formation.[32,33]

Additionally, the GATR study of these films – as for the films on SiO_2/Si (see Figure 6) – show that high anneal temperatures (> 700°C) are necessary to remove Lutetium dioxymonocarbonate species, indicated by the double peak at 1550 cm^{-1} and 1400 cm^{-1}. [35,36]

The SEM images (tilted view, 45°) of the Lu/Fe oxide films on Si_3N_4 are shown in Figure 9. Also in this case the formation of $Lu_2Si_2O_7$ in the film can be linked to a drastic morphology change: a PDA at 1100°C (see Figure 9d) results in a quite rough film, thus indicating crystalline silicate formation.

It has been shown that a phase-pure o-LFO film can be obtained via spin coating and subsequent annealing at 1000°C on $Si_3N_4/SiO_2/Si$ substrates. The dielectric constant of a 20 nm o-LFO film was investigated by means of impedance spectroscopy. Since the substrate is non-conducting , Au electrodes were deposited on the film. In order to obtain reliable results, the electrodes were deposited as a interdigitated structures, thus very close to each other. Via assumptions using the obtained impedance spectroscopy data, proposed by Kidner et al. [24], the dielectric constant (ε'), dielectric loss (ε'') and conductivity (σ) of the o-$LuFeO_3$ film were determined and plotted as a function of the frequency in Figure 10. It is clear that, for low frequencies, the dielectric constant is equal or higher than 10^4 (see Figure 10a). These measurements confirm, to the authors' knowledge for the first time, that the dielectric properties of bulk o-LFO [6] could be successfully transferred to the thin film variant. As can also be seen on the plot, the dielectric loss is quite high at low frequencies, while it decreases with the frequency, a kind of behavior typical for a slightly conductive material. This was also observed for the bulk material and it can possibly be linked to the origin of high permittivity. It is believed that it is due to charge separation, most likely in the inter-grain medium. When the blocking is not perfect, the current can still flow and this results in high losses at low frequencies.[6] At high frequencies there is a dispersion in conductivity (Figure 10b), which can be attributed to charge relaxation at inter-grain boundaries of the film. Furthermore, results from two different measurements reveal acceptable reproducibility of the electrical properties of the samples.

Conclusions

We developed a stable aqueous Lu/Fe precursor, which could be used for the synthesis of $LuFeO_3$ powders and for the chemical solution deposition of LFO thin films. Both the hexagonal and the orthorhombic phase could be obtained, depending on the post deposition anneal temperature, i.e. respectively 700°C and 1000°C for the films. Typically high temperatures were necessary, entering the zone of possible Lu silicate formation. This characteristic reaction of rare earth oxides with the substrate could be successfully delayed by the use of Si_3N_4 as protection layer. For the phase-pure o-LFO film on $Si_3N_4/SiO_2/Si$, to the authors' knowledge for the first time, a giant dielectric constant equal to or higher than 10^4 was shown for low frequencies (< 10^3 Hz), which makes it promising for the use in thin film capacitors.

Acknowledgments

The authors thank Bart Ruttens and Prof. Dr Jan D'Haen for powder x-ray diffraction measurements. The authors are also grateful to Dr Pieter Robaeys and Prof. Dr Milos Nesladek for lithography.

References

[1] A. Burke, Ultracapacitors : why, how, and where is the technology, J. Power Sources. 91 (2000) 37–50. doi:10.1016/S0378-7753(00)00485-7.

[2] B. Hudec, K. Husekova, E. Dobrocka, T. Lalinsky, J. Aarik, A. Aidla, et al., High-permittivity metal-insulator-metal capacitors with TiO2 rutile dielectric and RuO2 bottom electrode, IOP Conf. Ser. Mater. Sci. Eng. 8 (2010) 012024. doi:10.1088/1757-899X/8/1/012024.

[3] C. Zhu, B.-J. Cho, M.-F. Li, Atomic Layer Deposited High-κ Films and Their Role in Metal-Insulator-Metal Capacitors for Si RF/Analog Integrated Circuit Applications, Chem. Vap. Depos. 12 (2006) 165–171. doi:10.1002/cvde.200506393.

[4] J. Bird, Electrical and Electronic Principles and Technology, Fourth edi, Newnes - Elsevier, 2010.

[5] L.P. Zhu, H.M. Deng, L. Sun, J. Yang, P.X. Yang, J.H. Chu, Optical properties of multiferroic LuFeO3 ceramics, Ceram. Int. 40 (2014) 1171–1175. doi:10.1016/j.ceramint.2013.07.001.

[6] L. Zhang, X.M. Chen, Dielectric relaxation in LuFeO3 ceramics, Solid State Commun. 149 (2009) 1317–1321. doi:10.1016/j.ssc.2009.05.036.

[7] L. Zhu, H. Deng, J. Liu, L. Sun, P. Yang, Preparation and characterization of Bi-doped LuFeO3 thin films grown on LaNiO3 substrate, J. Cryst. Growth. 387 (2014) 6–9. doi:10.1016/j.jcrysgro.2013.10.039.

[8] W. Wang, J. Zhao, W. Wang, Z. Gai, N. Balke, M. Chi, et al., Room-temperature multiferroic hexagonal LuFeO3 films, Phys. Rev. Lett. 110 (2013) 237601. doi:10.1103/PhysRevLett.110.237601.

[9] W. Wang, H. Wang, X. Xu, L. Zhu, L. He, E. Wills, et al., Crystal field splitting and optical bandgap of hexagonal LuFeO3 films, Appl. Phys. Lett. 101 (2012) 241907. doi:10.1063/1.4771601.

[10] D. Khomskii, Classifying multiferroics: Mechanisms and effects, Physics (College. Park. Md). 2 (2009) 20. doi:10.1103/Physics.2.20.

[11] N.A. Spaldin, S.-W. Cheong, R. Ramesh, Multiferroics: Past, present, and future, Phys. Today. 63 (2010) 38. doi:10.1063/1.3502547.

[12] W. Eerenstein, N.D. Mathur, J.F. Scott, Multiferroic and magnetoelectric materials., Nature. 442 (2006) 759–65. doi:10.1038/nature05023.

[13] J.A. Moyer, R. Misra, J.A. Mundy, C.M. Brooks, J.T. Heron, D.A. Muller, et al., Intrinsic magnetic properties of hexagonal LuFeO3 and the effects of nonstoichiometry, APL Mater. 2 (2014) 012106. doi:10.1063/1.4861795.

[14] K. Kuribayashi, K. Nagashio, K. Niwata, M.S.V. Kumar, T. Hibiya, Novel criterion for formation of metastable phase from undercooled melt, Mater. Sci. Eng. A. 449-451 (2007) 675–679. doi:10.1016/j.msea.2006.02.430.

[15] L.P. Zhu, H.M. Deng, X.X. Li, P.X. Yang, J.H. Chu, Optical properties of LuFeO3 thin films prepared by pulsed laser deposition, J. Phys. Conf. Ser. 276 (2011) 012200. doi:10.1088/1742-6596/276/1/012200.

[16] A. Hardy, S. Van Elshocht, C. Adelmann, T. Conard, A. Franquet, O. Douhéret, et al., Aqueous solution–gel preparation of ultrathin ZrO2 films for gate dielectric application, Thin Solid Films. 516 (2008) 8343–8351. doi:10.1016/j.tsf.2008.04.017.

[17] S. Van Elshocht, A. Hardy, C. Adelmann, M. Caymax, T. Conard, A. Franquet, et al., Impact of Process Optimizations on the Electrical Performance of High-k Layers Deposited by Aqueous Chemical Solution Deposition, J. Electrochem. Soc. 155 (2008) G91. doi:10.1149/1.2840628.

[18] A. Hardy, S. Van Elshocht, W. Knaepen, J. D'Haen, T. Conard, B. Brijs, et al., Crystallization resistance of barium titanate zirconate ultrathin films from aqueous CSD: a study of cause and effect, J. Mater. Chem. 19 (2009) 1115. doi:10.1039/b816856c.

[19] A. Hardy, S. Van Elshocht, J. D'Haen, O. Douhéret, S. De Gendt, M. Caymax, et al., Aqueous chemical solution deposition of ultrathin lanthanide oxide dielectric films, J. Mater. Res. 22 (2007) 3484–3493. doi:10.1557/JMR.2007.0433.

[20] D. Dewulf, N. Peys, S. Van Elshocht, G. Rampelberg, C. Detavernier, S. De Gendt, et al., Interfacial reactions of Gd- and Nb-oxide based high-k layers deposited by aqueous chemical solution deposition, Microelectron. Eng. 88 (2011) 1338–1341. doi:10.1016/j.mee.2011.03.045.

[21] A. Hardy, S. Gielis, H. Van den Rul, J. D'Haen, M.K. Van Bael, J. Mullens, Effects of precursor chemistry and thermal treatment conditions on obtaining phase pure bismuth ferrite from aqueous gel precursors, J. Eur. Ceram. Soc. 29 (2009) 3007–3013. doi:10.1016/j.jeurceramsoc.2009.05.018.

[22] M.K. Van Bael, D. Nelis, A. Hardy, D. Mondelaers, K. Van Werde, J. D'Haen, et al., Integrated Ferroelectrics : An Aqueous Chemical Solution Deposition of Ferroelectric Thin Films, Integr. Ferroelectr. 45 (2002) 113–122. doi:10.1080/10584580215353.

[23] J.R. Vig, Treatise on Clean Surface Technolgy - Volume 1, 1st ed., Plenum Press, New York, 1987.

[24] N.J. Kidner, Z.J. Homrighaus, T.O. Mason, E.J. Garboczi, Modeling interdigital electrode structures for the dielectric characterization of electroceramic thin films, Thin Solid Films. 496 (2006) 539–545. doi:10.1016/j.tsf.2005.08.350.

[25] K. Van Werde, D. Mondelaers, G. Vanhoyland, D. Nelis, M.K. Van Bael, J. Mullens, et al., Thermal decomposition of the ammonium zinc acetate citrate precursor for aqueous chemical solution deposition of ZnO, J. Mater. Sci. 37 (2002) 81–88. doi:10.1023/A:1013141723764.

[26] A. Hardy, K. Van Werde, G. Vanhoyland, M.K. Van Bael, J. Mullens, L.C. Van Poucke, Study of the decomposition of an aqueous metal – chelate gel precursor for (Bi,La)4Ti3O12 by means of TGA – FTIR , TGA – MS and HT-DRIFT, Thermochim. Acta. 397 (2003) 143–153. doi:10.1016/S0040-6031(02)00272-1.

[27] D. Nelis, D. Mondelaers, G. Vanhoyland, A. Hardy, K. Van Werde, H. Van Den Rul, et al., Synthesis of strontium bismuth niobate (SrBi2Nb2O9) using an aqueous acetate–citrate precursor gel: thermal decomposition and phase formation, Thermochim. Acta. 426 (2005) 39–48. doi:10.1016/j.tca.2004.07.005.

[28] N. Peys, Y. Ling, D. Dewulf, S. Gielis, C. De Dobbelaere, D. Cuypers, et al., V6O13 films by control of the oxidation state from aqueous precursor to crystalline phase, Dalt. Trans. 42 (2013) 959–968. doi:10.1039/c2dt31857a.

[29] V.I. Trofimov, I. V. Trofimov, J.-I. Kim, The effect of finite film thickness on the crystallization kinetics of amorphous film and microstructure of crystallized film, Thin Solid Films. 495 (2006) 398–403. doi:10.1016/j.tsf.2005.08.221.

[30] S. Van Elshocht, C. Adelmann, T. Conard, A. Delabie, A. Franquet, L. Nyns, et al., Silicate formation and thermal stability of ternary rare earth oxides as high-k dielectrics, J. Vac. Sci. Technol. A Vacuum, Surfaces, Film. 26 (2008) 724. doi:10.1116/1.2891257.

[31] K. Ishikawa, Y. Uchiyama, H. Ogawa, S. Fujimura, Dependence of TO and LO mode frequency of thermally grown silicon dioxide films on annealing temperature, Appl. Surf. Sci. 117/118 (1997) 212–215. doi:10.1016/S0169-4332(97)80081-5.

[32] H. Ono, T. Katsumata, Interfacial reactions between thin rare-earth-metal oxide films and Si substrates, Appl. Phys. Lett. 78 (2001) 1832. doi:10.1063/1.1357445.

[33] H. Ohashi, M.D. Alba, A.I. Becerro, P. Chain, A. Escudero, Structural study of the Lu2Si2O7–Sc2Si2O7 system, J. Phys. Chem. Solids. 68 (2007) 464–469. doi:10.1016/j.jpcs.2006.12.025.

[34] N. Rochat, A. Chabli, F. Bertin, C. Vergnaud, P. Mur, S. Petitdidier, et al., Infrared analysis of thin layers by attenuated total reflection spectroscopy, Mater. Sci. Eng. B. 102 (2003) 16–21. doi:10.1016/S0921-5107(02)00749-3.

[35] T. Gougousi, M.J. Kelly, D.B. Terry, G.N. Parsons, Properties of La-silicate high-K dielectric films formed by oxidation of La on silicon, J. Appl. Phys. 93 (2003) 1691. doi:10.1063/1.1531818.

[36] D. Dewulf, A. Hardy, S. Van Elshocht, C. De Dobbelaere, W.C. Wang, M. Badylevich, et al., Gadolinium -niobates and -tantalates: Amorphous High-k Materials by Aqueous CSD, J. Electrochem. Soc. 159 (2012) G75. doi:10.1149/2.072206jes.

[37] J.H. Kim, K.W. Chung, Microstructure and properties of silicon nitride thin films deposited by reactive bias magnetron sputtering, J. Appl. Phys. 83 (1998) 5831. doi:10.1063/1.367440.

[38] E.A. Taft, Characterization of Silicon Nitride Films, J. Electrochem. Soc. 118 (1971) 1341. doi:10.1149/1.2408318.

[39] N. Wada, S.A. Solin, J. Wong, S. Prochazka, Raman and IR absorption spectroscopic studies on alfa, beta and amorphous Si3N4, J. Non. Cryst. Solids. 43 (1981) 7–15. doi:10.1016/0022-3093(81)90169-1.

[40] V. Tsu, G. Lucovsky, M.J. Mantini, Local atomic structure in thin films of silicon nitride and silicon diimide produced by remote plasma-enhanced chemical-vapor deposition, Phys. Rev. B. 33 (1986) 7069–7076. doi:10.1103/PhysRevB.33.7069.

[41] K.O. Bugaev, A.A. Zelenina, V.A. Volodin, Vibrational Spectroscopy of Chemical Species in Silicon and Silicon-Rich Nitride Thin Films, Int. J. Spectrosc. 2012 (2012) 1–5. doi:10.1155/2012/281851.

[42] JCPDS, Powder Diffraction File of Inorganic Phases, Joint Committee on Powder Diffraction Standards, Swarthmore, (1997).

Figure captions

Figure 1: Synthesis flowchart of the Lu/Fe precursor, powder and thin films.

Figure 2: TGA and DTG (10°C/min, 100 ml/min in dry air) of the Lu/Fe citrate gel.

Figure 3: HT-XRD patterns of the Lu/Fe citrate gel at the temperatures indicated in air. As a reference the XRD signals originating from hexagonal (⎔) and orthorhombic (★) $LuFeO_3$ are shown.[42]

Figure 4: (a) Plot of the film thickness of Lu/Fe oxide films, determined via spectroscopic ellipsometry, as a function of the amount of deposition cycles (i.e. spin coating and subsequent thermal treatment on hot plates) and (b) X-SEM image of the Lu/Fe oxide film after 16 deposition cycles

Figure 5: XRD patterns of ca. 130 nm Lu/Fe films on SiO_2/Si, deposited via spin coating and crystallized via a post deposition anneal in dry air at the temperatures indicated. As a reference the XRD signals originating from hexagonal $LuFeO_3$ (⎔), $Lu_2Si_2O_7$ (▽) and hexagonal Fe_2O_3 (⬣) are shown.[42]

Figure 6: GATR spectra of ca. 130 nm Lu/Fe films on SiO_2/Si, deposited via spin coating and crystallized by a post deposition anneal in dry air at the temperatures indicated. As guidance, the identification of the peaks is shown.

Figure 7: SEM images (tilted view, 45°) of ca. 130 nm Lu/Fe films on SiO_2/Si, deposited via spin coating and crystallized via a post deposition anneal in dry air at (a) 800°C, (b) 900°C, (c) 1000°C and (d) 1100°C.

Figure 8: GATR spectra of ca. 65 nm Lu/Fe films on Si_3N_4/SiO_2/Si, deposited via spin coating and crystallized via a post deposition anneal in dry air at the temperatures indicated. As guidance, the identification of the peaks is shown.

Figure 9: SEM images (tilted view, 45°) of ca. 65 nm Lu/Fe films on Si_3N_4/SiO_2/Si, deposited via 10 cycles of spin coating and crystallized via a post deposition anneal in dry air at (a) 800°C, (b) 900°C, (c) 1000°C and (d) 1100°C.

Figure 10: Plot of the (a) dielectric constant (ε'), dielectric loss (ε'') and (b) conductivity (σ) of a 20 nm o-$LuFeO_3$ film, determined via impedance spectroscopy. For the measurement Au electrodes were deposited on the film as interdigitated finger structures.

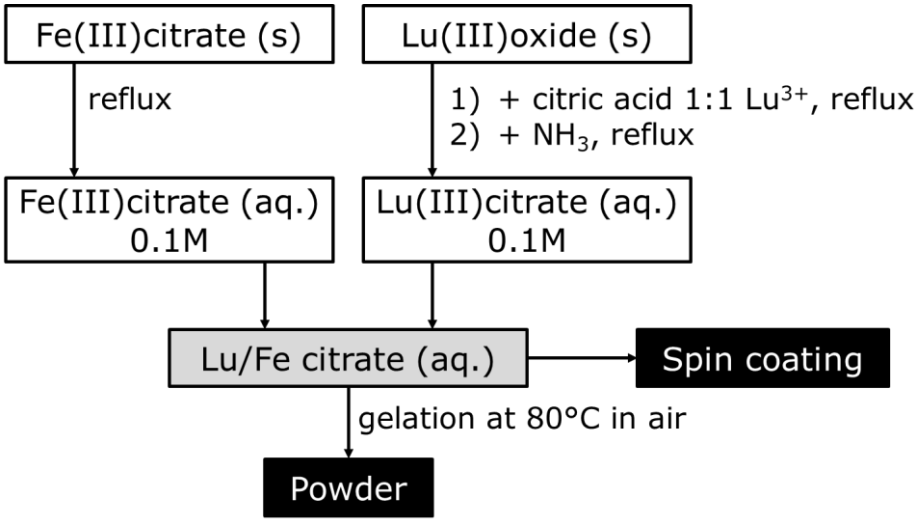

Figure 1: Synthesis flowchart of the Lu/Fe precursor, powder and thin films.

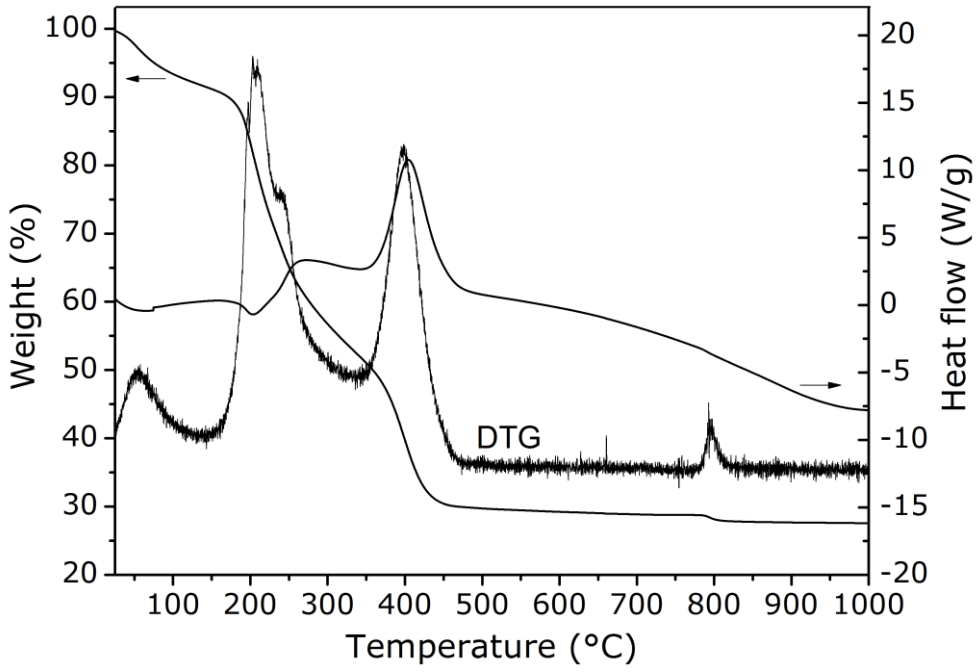

Figure 2: TGA and DTG (10°C/min, 100 ml/min in dry air) of the Lu/Fe citrate gel.

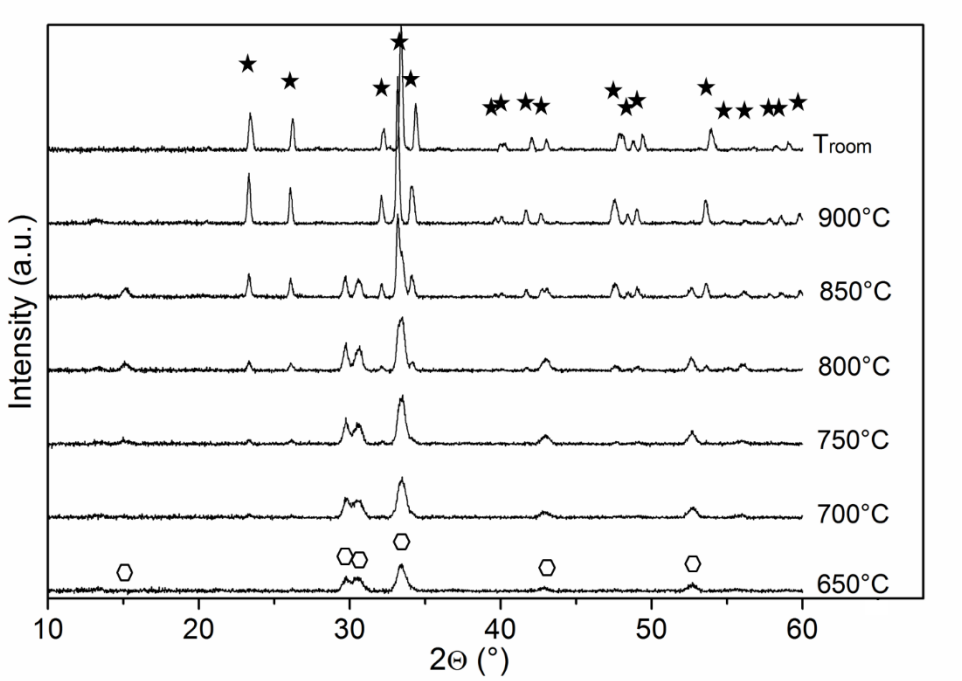

Figure 3: HT-XRD patterns of the Lu/Fe citrate gel at the temperatures indicated in air. As a reference the XRD signals originating from hexagonal (⬡) and orthorhombic (★) $LuFeO_3$ are shown.[42]

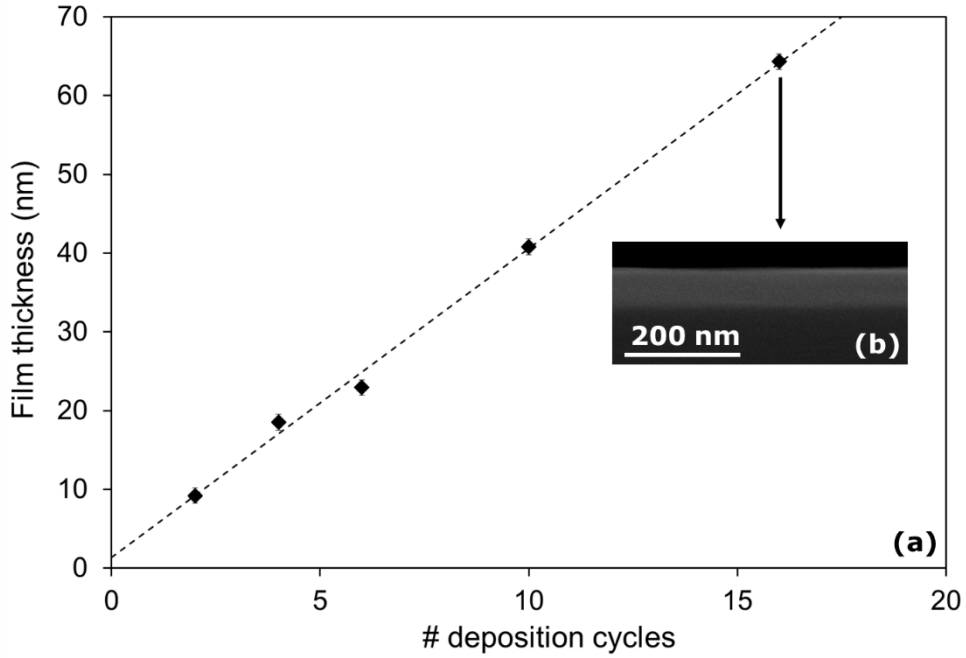

Figure 4: (a) Plot of the film thickness of Lu/Fe oxide films, determined via spectroscopic ellipsometry, as a function of the amount of deposition cycles (i.e. spin coating and subsequent thermal treatment on hot plates) and (b) X-SEM image of the Lu/Fe oxide film after 16 deposition cycles

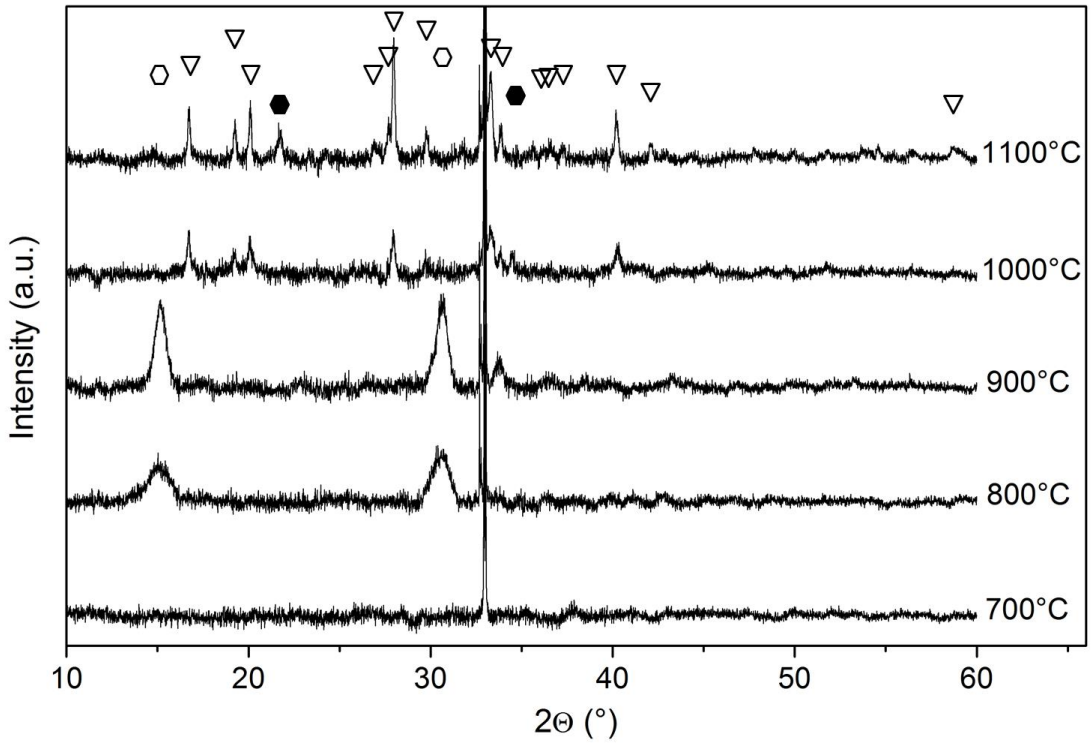

Figure 5: XRD patterns of ca. 130 nm Lu/Fe films on SiO_2/Si, deposited via spin coating and crystallized via a post deposition anneal in dry air at the temperatures indicated. As a reference the XRD signals originating from hexagonal $LuFeO_3$ (⬡), $Lu_2Si_2O_7$ (▽) and hexagonal Fe_2O_3 (⬢) are shown.[42]

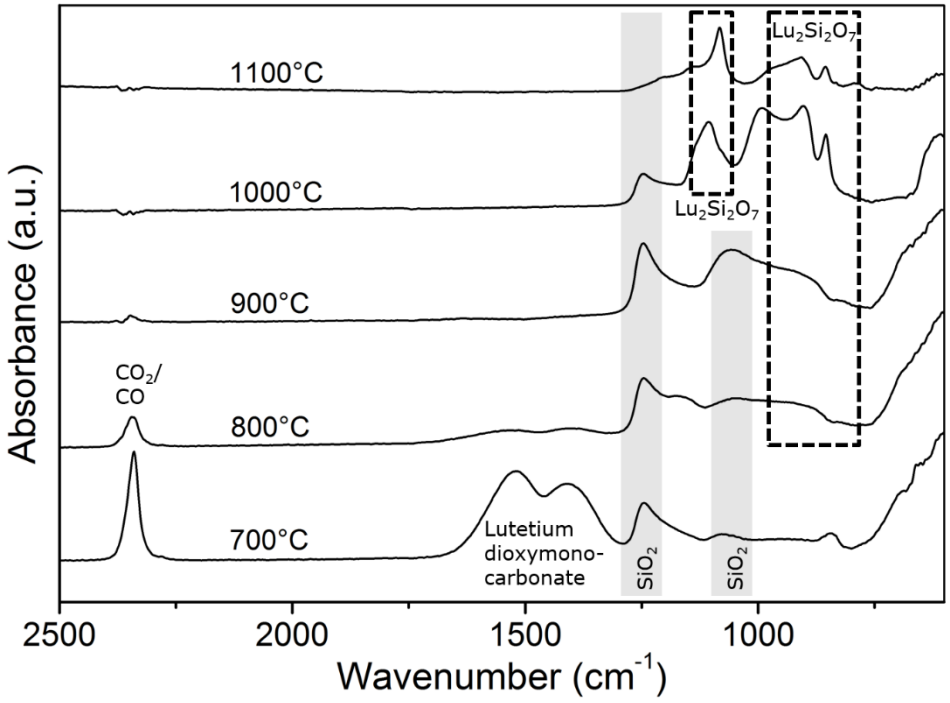

Figure 6: GATR spectra of ca. 130 nm Lu/Fe films on SiO_2/Si, deposited via spin coating and crystallized by a post deposition anneal in dry air at the temperatures indicated. As guidance, the identification of the peaks is shown.

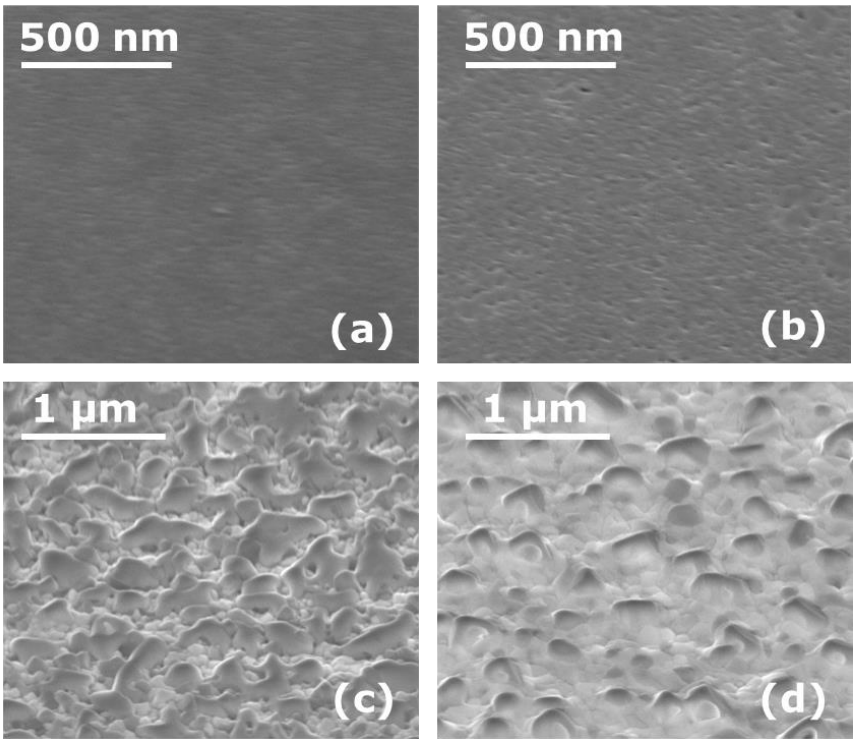

Figure 7: SEM images (tilted view, 45°) of ca. 130 nm Lu/Fe films on SiO_2/Si, deposited via spin coating and crystallized via a post deposition anneal in dry air at (a) 800°C, (b) 900°C, (c) 1000°C and (d) 1100°C.

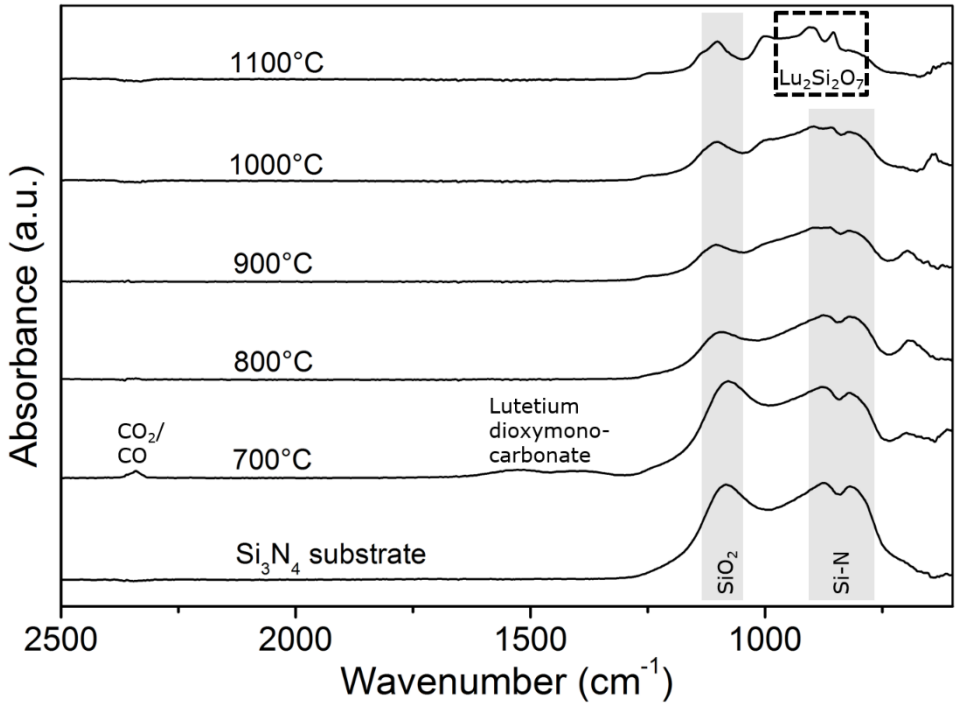

Figure 8: GATR spectra of ca. 65 nm Lu/Fe films on $Si_3N_4/SiO_2/Si$, deposited via spin coating and crystallized via a post deposition anneal in dry air at the temperatures indicated. As guidance, the identification of the peaks is shown.

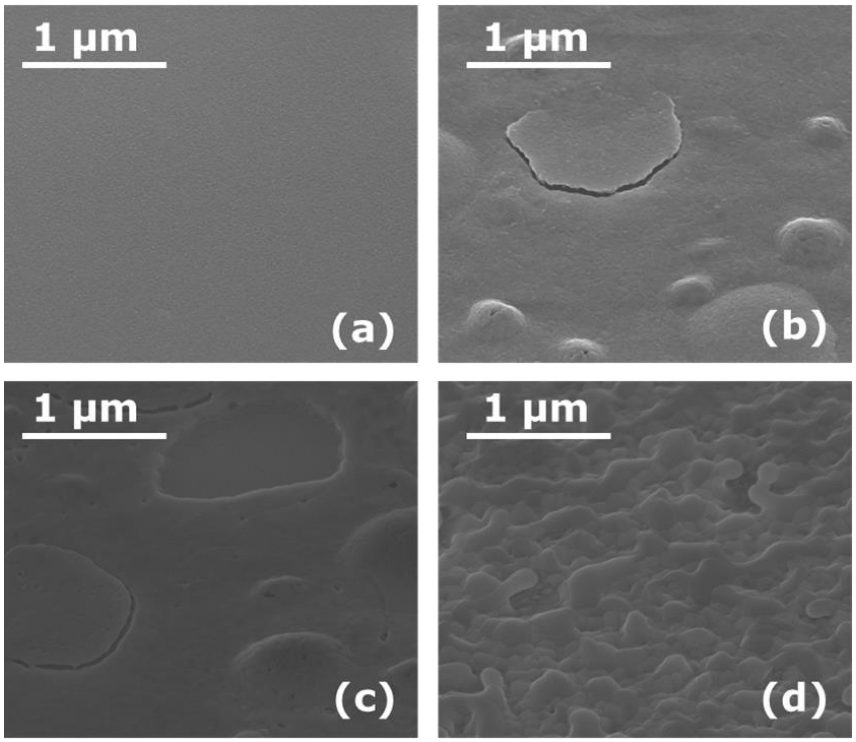

Figure 9: SEM images (tilted view, 45°) of ca. 65 nm Lu/Fe films on $Si_3N_4/SiO_2/Si$, deposited via 10 cycles of spin coating and crystallized via a post deposition anneal in dry air at (a) 800°C, (b) 900°C, (c) 1000°C and (d) 1100°C.

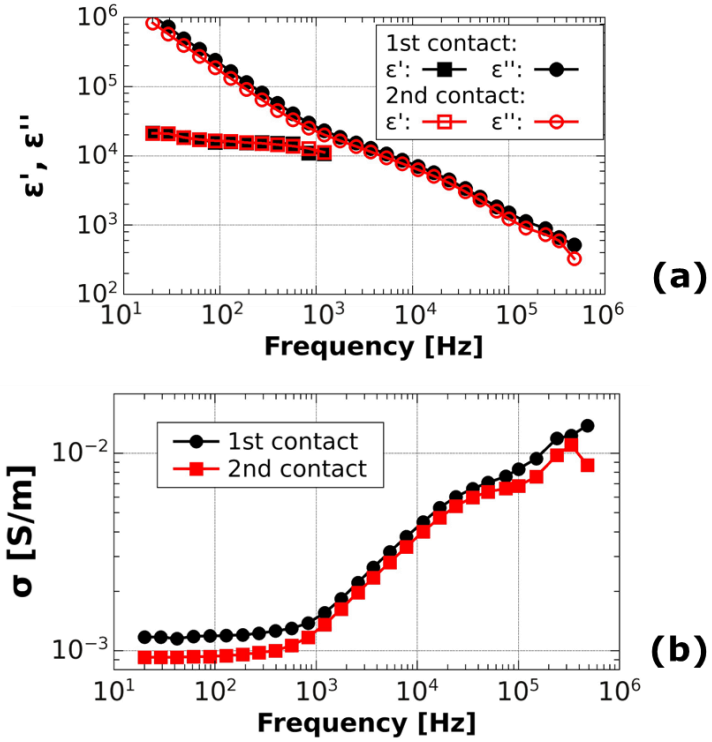

Figure 10: Plot of the (a) dielectric constant (ε'), dielectric loss (ε'') and (b) conductivity (σ) of a 20 nm o-$LuFeO_3$ film, determined via impedance spectroscopy. For the measurement Au electrodes were deposited on the film as interdigitated finger structures.